Bull Volcanol (2000) 62 : 331–346
DOI 10.1007/s004450000103

RESEARCH ARTICLE

A. M. F. Lagmay · B. van Wyk de Vries · N. Kerle
D. M. Pyle

Volcano instability induced by strike-slip faulting

Received: 29 November 1999 / Accepted: 29 July 2000 / Published online: 15 September 2000

Abstract Analogue sand cone experiments were conducted to study instability generated on volcanic cones by basal strike-slip movement. The results of the analogue models demonstrate that edifice instability may be generated when strike-slip faults underlying a volcano move as a result of tectonic adjustment. This instability occurs on flanks of the volcano above the strike-slip shear. On the surface of the volcano this appears as a pair of sigmoids composed of one reverse and one normal fault. In the interior of the cone the faults form a flower structure. Two destabilised regions are created on the cone flanks between the traces of the sigmoidal faults. Bulging, intense fracturing and landsliding characterise these unstable flanks. Additional analogue experiments conducted to model magmatic intrusion show that fractures and faults developed within the volcanic cone due to basal strike-slip motions strongly control the path of the intruding magma. Intrusion is diverted towards the areas where previous development of reverse and normal faults have occurred, thus causing further instability. We compare our model results to two examples of volcanoes on strike-slip faults: Iriga volcano (Philippines), which underwent non-magmatic collapse, and Mount St. Helens (USA), where a cryptodome was emplaced prior to failure. In the analogue and natural examples, the direction of collapse takes place roughly parallel to the orientation of the underlying shear. The model presented proposes one mechanism for strike-parallel breaching of volcanoes, recently recognised as a common failure direction of volcanoes found in regions with transcurrent and transtensional deformation. The recognition of the effect of basal shearing on volcano stability enables prediction of the likely direction of eventual flank failure in volcanoes overlying strike-slip faults.

Keywords Volcano instability · Deformation · Sector collapse · Strike-slip faulting · Mount St. Helens · Iriga · Analogue modelling

Editorial responsibility: S. Carey

A. M. F. Lagmay (✉) · D. M. Pyle
Department of Earth Sciences, University of Cambridge, Downing Street, Cambridge, CB2 3EQ UK
E-mail: mlagmay@nigs.cs.upd.edu.ph; amfal2@esc.cam.ac.uk
Phone: +632-9290647

A. M. F. Lagmay
National Institute of Geological Sciences, University of the Philippines, C.P. Garcia Street, Diliman, Quezon City 1104, Philippines

B. van Wyk de Vries
Laboratoire Magmas et Volcans, Université Blaise Pascal, 5 rue Kessler, 63038 Clermont-Ferrand, France

N. Kerle
Department of Geography, University of Cambridge, Downing Place, CB2 3EN, UK

Introduction

Active volcanoes are dynamic structures characterised by continued growth marked with episodes of instability that lead to structural failure (e.g. landslides and large avalanches). Edifice instability may occur in response to any of several factors, including steepening of slopes (Siebert 1984; Begét and Kienle 1992), flank overloading from tephra and lava accumulation (Shteynberg and Solov'yev 1976; Murray 1988), magma intrusion (Swanson et al. 1976; Moriya 1980; Christiansen and Peterson 1981; Elsworth and Voight 1996), hydrothermal activity (Lopez and Williams 1993; Day 1996; Voight and Elsworth 1997), peripheral erosion during sea-level changes (Guest et al. 1988; Moore and Clague 1992; Blanchon and Shaw 1995; Firth et al. 1996), gravitational spreading (Borgia 1994; Merle and Borgia 1996; van Wyk de Vries and Francis 1997; van Wyk de Vries and Matela 1998) and tectonic movement (Francis and Self 1987; Carracedo

1994; Tibaldi 1995). Instability can develop over a long period of time, in the range of thousands of years (Nakamura 1982; Stewart et al. 1993; McGuire et al. 1996; Murray and Voight 1996), or can occur over a short interval, within a few days or a few months (Christiansen and Peterson 1981; Belousov 1996). Slow development of instability is incremental (Ridley 1971; Swanson et al. 1976; McGuire and Pullen 1989; van Wyk de Vries and Francis 1997) and results from the progressive and cumulative effects of individual destabilising events (e.g. dike intrusion in Etna and Kilauea). In the case of rapid destabilisation, the cause may be due to a discrete event such as cryptodome emplacement (e.g. Mount St. Helens in 1980) or a large seismic shock. A slowly developing instability may accelerate with a discrete event and culminate in catastrophic edifice failure.

Previous models which attempted to relate volcano morphology to the regional tectonic stress field were developed by Nakamura (1977), Moriya (1980) and Siebert (1984). Nakamura proposed that cone elongation, strike of dikes (fractures) and alignment of flank vents occur parallel to the regional maximum compressive stress direction (σ_{Hmax}). Nakamura's (1977) model was later used by Moriya (1980) to explain the perpendicular relationship between the orientation of amphitheatre craters and the regional σ_{Hmax} stress direction (Fig. 1a) observed in 30 volcanoes of Japan. Moriya (1980) postulated that the steeper slopes normal to the elongation direction of the volcano, the strengthening of volcanic flanks parallel to dike emplacement, and the dilational effect of dike intrusion promotes failure perpendicular to the σ_{Hmax} direction. Siebert (1984) adds that in Japan, which has the highest documented number of avalanche calderas, a much higher percentage of volcanoes with parallel dike swarms have formed amphitheatre-like calderas than have volcanoes without a dominant direction of dike orientation. He suggested that dike swarms which develop parallel to the regional σ_{Hmax} play an important role in volcanic slope failure.

Not all volcanoes, however, show the similar response to tectonic stress suggested by Moriya (1980). In many cases volcanoes show cylindrical vent systems with widely varying dike orientations (Siebert 1984). In some cases dikes are not present at all. Morever, Nakamura's model (1977), when applied to Indonesian volcanoes, was found not to be consistent with the regional σ_{Hmax} stress direction (Bahar and Girod 1983). Bahar and Girod (1983) showed that, in many cases, the alignment of volcanoes, dikes and flank vents tended to form at an angle, typically a high angle relative to σ_{Hmax} (determined from regional fault-and-fold structures). These observations indicate that the response of volcanoes to the regional stress can be less straightforward than envisaged by Nakamura (1977) and Moriya (1980). Fracture planes are used as pathways by magma in complex ways relative to the regional stress field (Delaney et al. 1986; Pasquaré et al. 1988). This means that in terms of cone morphology, including that of cone breaching or collapse, volcanoes can respond to the regional stress in a variety of ways. More recently, Tibaldi (1995) showed that it is possible to determine the regional state of stress from cone morphology and fracture patterns, provided that it is done with care. Usually, earthquake fault-plane mechanisms are used together with observations of surface fault patterns to accurately determine buried brittle tectonics and the principal stress orientation of the region (Weaver et al. 1987).

Francis and Wells (1988) examined 28 examples of breached cones in the Central Andes. They found that most breaching occurred approximately perpendicular to the direction of the resultant vector of observed structural lineaments (i.e. fractures). The resultant vector in the Central Andes trends 011°, which means that collapse occurs roughly parallel to the regional thrust vergence (Munoz and Charrier 1996; i.e. roughly parallel to σ_{Hmax}).

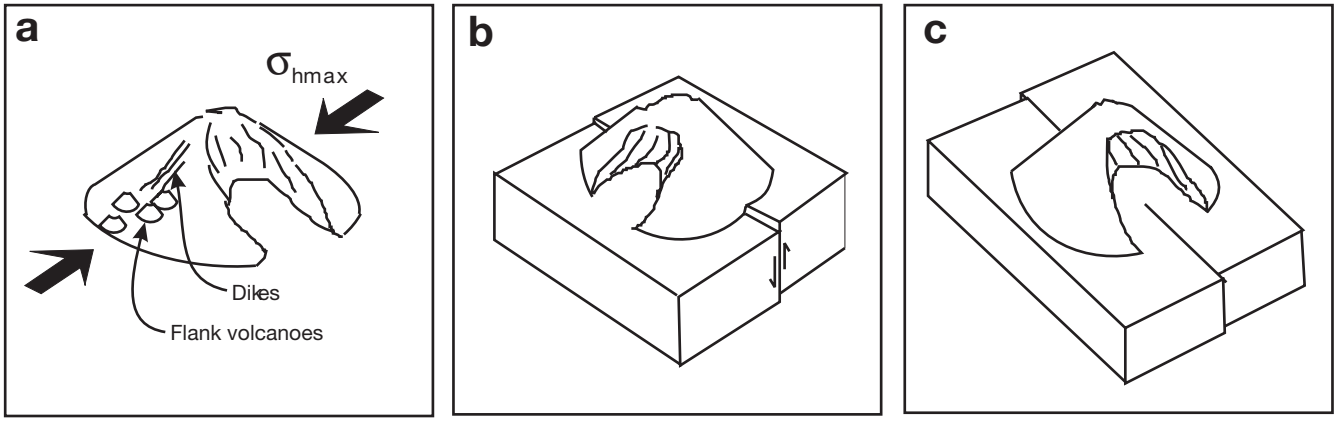

Fig. 1a–c Breaching models that relate the direction of flank failure to the regional stress field or underlying fault structure. **a** Moriya's (1980) model relates flank failure perpendicular to the regional maximum horizontal compressive stress direction (σ_{hmax}). **b** Fault-perpendicular breach of the volcano. Failure is in the dip direction of the normal fault. **c** Fault-parallel breach of the volcano. The underlying fault can be dip-slip or strike-slip

Tibaldi (1995) examined 1315 Quaternary volcanoes in different structural settings to establish the nature of the relationship between volcano morphology and tectonic setting. He found that cone breaching perpendicular to the fault strike (Fig. 1b) was more prevalent in extensional regions than in other settings. Volcanoes in such settings usually collapse in the direction of the downthrown block (Vidal and Merle 2000). In contrast, breaching parallel to the fault strike (Fig. 1c) is more common in regions with transcurrent or transtensional tectonics (Tibaldi 1995).

Whereas breaching perpendicular to the strike of faults underlying volcanic cones can be explained either by the geometry of normal faults (Tibaldi 1995) or strengthening of the regions parallel to dike emplacement (Moriya 1980), mechanisms for fault-parallel breaching or collapse are poorly understood. One possible contributory factor is the presence of sloping substrate, dipping in the strike direction of the underlying fault. Another is lateral spreading (van Wyk de Vries and Merle 1996) in extensional and transtensional regions, which favours flank failure parallel to the faults formed within the volcano. To our knowledge, no mechanisms have been proposed for strike-parallel failure in volcanoes on top of transcurrent (strike-slip) faults.

Motivation and objectives

The motivation for this work arose from the observation that volcanoes nested on top of strike-slip fault zones often develop prominent sector collapse scars. A list of selected examples documented in the volcanology literature is presented in Table 1.

Two examples are studied in detail in this work: Iriga volcano, Philippines, and Mount St. Helens, USA (see Fig. 2). Edifice failure of Iriga volcano occurred without an accompanying magmatic inrusion (Aguila et al. 1986). At Mount St. Helens, sector collapse was aided by cryptodome emplacement (Christiansen and Peterson 1981). In both these cases the amphitheatre scars trend roughly parallel to the strike-slip faults. Because of this geometric relationship, we make the hypothesis that this results from the effect of strike-slip fault movement on edifice stability. We test this causal relationship between tectonic (strike-slip) movement and volcanic flank failure by comparative analysis of morphometric features found in digital elevation models (DEM) of Iriga with those developed in laboratory analogue cones. For Mount St. Helens, detailed structural (Moore and Albee 1981; Jordan and Kieffer 1981) and geodetic data (Lipman et al. 1981) relating to the 1980 collapse event provide a unique opportunity for evaluating this hypothesis.

We explore the effects of strike-slip faulting underneath volcanoes, and its role in inducing instability in volcanic structures over a wide range of timescales. Analogue modelling is used to determine how brittle deformation occurs in volcanic cones above strike-slip faults by identifying the types of structures developed, their magnitude, location, and rates and extent of propagation. The objectives are to identify zones of structural weakness and steepened slopes, the areas with greatest potential for failure (Christiansen and

Table 1 Examples of volcanoes on strike-slip faults

Name of volcano	Location	Fault name	Fault trend	Breach direction	Reference
Mount St. Helens	USA	MSH shear	NNW	N	Weaver et al. (1987)
Iriga	Philippines	Legaspi fault	NW–SE	SE	This study
Vesuvius	Italy		NE–SW	Somma open to SW	Marzocchi et al. (1993)
Vulture	Italy			W	Guest et al. (1988)
Lipari	Italy	Tindari-Letojanni Fault	NNW	N ; S	Ventura (1994)
Volcano	Italy	Tindari-Letojanni Fault	NNW	NW ; NNE	Ventura (1994)
Salina	Italy	Tindari-Letojanni Fault	NNW	NW ; N	Ventura (1994)
Kara Dag	Turkey			NW	Dhont et al. (1998)
Mombacho	Nicaragua	Ochomogo Fault	NE–SW	NE ; S ; SE	Van Wyk de Vries and Francis (1997)
Soputan	Sulawesi		ENE		Van Wyk de Vries and Merle (1998)
Gunung Lokon	Sulawesi		ENE		Van Wyk de Vries and Merle (1998)
Hasan Dag	Turkey	Tuz Golu			Pasquaré et al. (1988)
Erciyes Dag	Turkey	Ecemis			Pasquaré et al. (1988)
Suphan	Turkey	Suphan Fault	NE		Adiyaman et al. (1998)
Cayambe	Ecuador	Cayambe-Chingual	NE		Tibaldi (1992)
Chimborazo	Ecuador		NNE		Tibaldi (1992)
Soche	Ecuador		NE		Tibaldi (1992)
Zapatera	Nicaragua	Ochomogo Fault	NE–SW		Van Wyk de Vries (1988)
Telica	Nicaragua		SE		Weinberg (1992)
Cerro Negro	Nicaragua		SE		Weinberg (1992)
Nevado Sabancaya	Peru				Vandemeulebrouck, (pers. commun.)

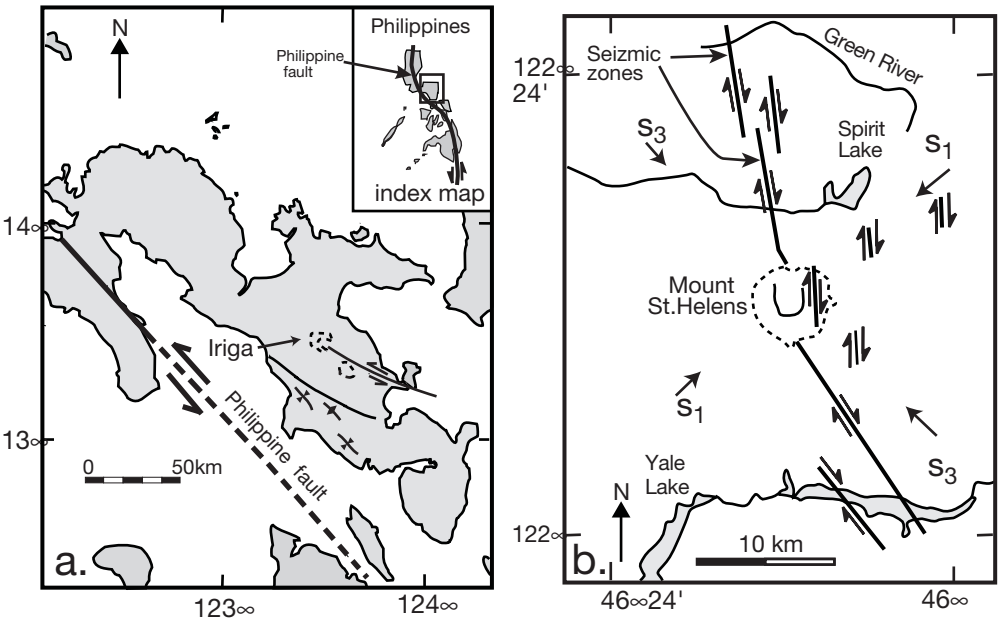

Fig. 2a,b Examples of volcanoes sitting on strike-slip faults. **a** At the right of centre of the map is Iriga volcano. A left-lateral strike-slip fault cuts underneath the volcano. *Index map* shows the location of southeastern Luzon (*grey box*) and the left-lateral Philippine fault. Modified from Aguila et al. (1986). **b** Mount St. Helens with a right-lateral strike-slip fault beneath the edifice. The faults north of Mount St. Helens trend N8°W, shifting towards a N35°W orientation in the southern portion. Also shown is the regional stress direction. (**b** adapted from Weaver et al. 1987)

Peterson 1981; Duffield et al. 1982; Siebert 1984; Begét and Kienle 1992). In terms of rapid destabilisation, as in the case of magmatic intrusion, we evaluate how brittle deformation influences the path of magma.

From a hazards perspective, the numerous examples of volcanoes nested on strike-slip faults, and the recognition of the dominance of fault-parallel breaching in transcurrent and transtensional regions (Tibaldi 1995), shows the need to investigate this class of volcanoes. We show how analysis of the regional stress field and structures found on volcanic flanks may be used to predict the collapse direction of volcanoes built on top of strike-slip faults.

Methods

Experimental procedure

Brittle strike-slip without intrusion

To determine how strike-slip faulting affects volcanic-edifice stability, an analogue model of a cone on a sheared basal layer was used. This model is similar to the experimental set-up of van Wyk de Vries and Merle (1998). Both left-lateral and right-lateral shear movement of the base are simulated in the models. The set-up is shown in Fig. 3.

The experimental apparatus comprises a basal plate attached to a vertical sideplate fastened to a screwjack. Rotation of the screwjack is controlled by a computer. Counterclockwise motion of the screwjack causes the basal plate to move, thus generating left-lateral and right-lateral shears at its lengthwise margins. Dry sand cones were placed on the side of the basal plate. The sizes of the cones were variable and ranged in height from 4 to 6 cm. Each cone was built at its maximum angle of repose. The cone is composed of a mixture of sieved sand (3–5 μm) and plaster. The plaster was added to make the material more cohesive. In some experiments, a pure sand layer (substrate) 5 cm thick with plan view dimensions of 50×43 cm was laid on the basal plate.

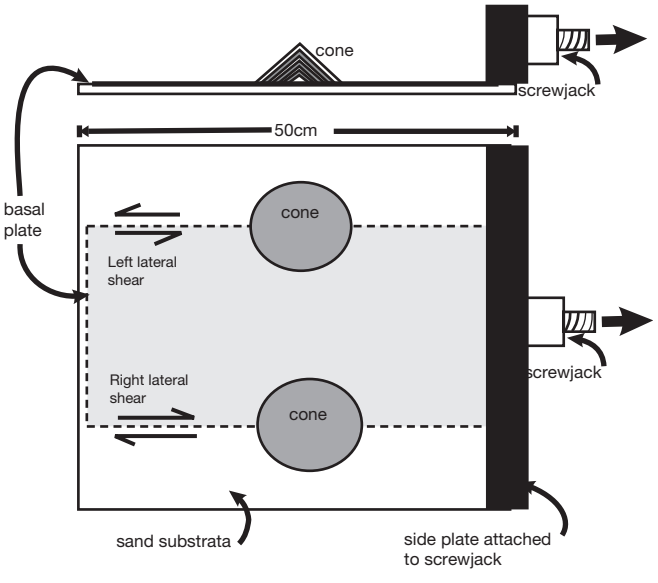

Fig. 3 Side and plan views of the analogue model, showing the substrate layer of sand and cones which represent volcanic edifices. The layer of sand (5 cm thick) rests on top of a basal plate of cardboard (1 mm thick) which is attached to a sideplate. The sideplate is pulled by a screwjack, which moves according to a desired rate specified by a computer. Strike-slip shearing is generated along the margins of the basal plate when the screwjack is pulled

Intrusion experiments

An additional series of experiments were conducted to study the effect of magma intrusion into a strike-slip faulted volcano. A set-up similar to the aforementioned set-up was used, but with an intrusion apparatus placed directly below the cone summit. This additional procedure in the model set-up was the same as that used in the experiments of Donnadieu and Merle (1998). The viscous magma analogue is silicone putty.

In the intrusion models, the following sets of experiments were carried out:

1. Several experiments were run with no strike-slip motion to show that the cryptodome intrudes at random orientations in the cone.
2. The cone was faulted by strike-slip motion and then halted before simulating the intrusion. This left the cone fractured. Variable amounts of shear were applied before intrusion, and the rates of intrusion were also varied.
3. The cone was faulted as in item 2, and the motion was allowed to continue during intrusion.

Our scaling did not permit us to model the slow rates of motion envisaged for the Mount St. Helens shear zone. The slowest motion rate in the simulations was equivalent to approximately 0.63 m per year. While this is not unreasonable for a strike-slip fault, especially during periods of high seismic activity, no such movement was described during the 1980 Mount St. Helens event.

Analytical methods

The analogue experiments were photographed to record structures developed as a result of progressive strike-slip movement. Completed experiments were wetted and then sliced perpendicular to the shear zone and horizontally (parallel to the substrate). This was done to reveal in three dimensions the deformational structures within the cone.

The results of the experiments were compared with digital elevation models (DEM) of Iriga and Mount St. Helens volcanoes. The DEM of Iriga volcano was generated using digital photogrammetry of 1:25,000-scale aerial photographs and has a spatial resolution of 10 m. The April to May pre-eruption DEM images of Mount St. Helens are from Jordan and Kieffer (1981). Geodetic data from Lipman et al. (1981), and structural observations from Moore and Albee (1981), were used to augment the information collected from DEMs.

Geometric, dynamic and kinematic similarities with the natural prototype were observed in the experimental set-up. The scaling procedure was the same as those presented in previous analogue experiments on the deformation of volcanic edifices (Merle and Vendeville 1995; Merle and Borgia 1996; van Wyk de Vries and Merle 1996; van Wyk de Vries and Merle 1998; Donnadieu and Merle 1998; van Wyk de Vries et al. 2000). The properties used in scaling of the model with the natural prototype are listed in Tables 2 and 3, and a diagram of the apparatus in Fig. 4.

Table 2 Model material and natural prototype properties

	Density (ρ) (kg m^{-3})	Cohesion τ_0 (Pa)	Angle of friction ϕ (°)	Viscosity μ (Ps s)
Sand	1400	0	30–35	-
Sand/plaster	1300	25–250	30–40	-
Silicone	1000	-	-	4×10^4
Brittle rock	2500	0–10^7	30–40	-

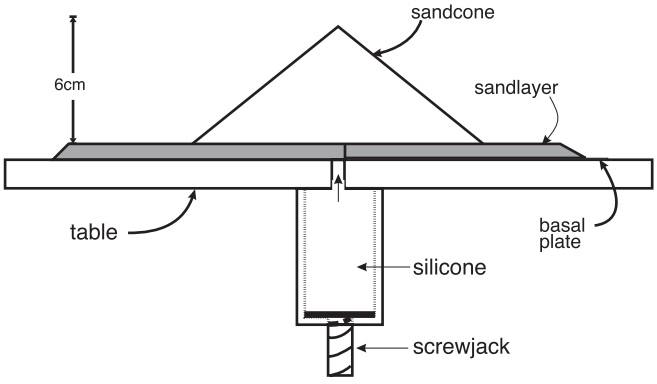

Fig. 4 Set-up of the intrusion model of a sheared cone. The cardboard basal plate is used to shear the cone. The screwjack controls the rate of injection of the silicone into the cone

Table 3 Model scaling factors

	Model	Nature	Ratio (model/nature)
Length (height of volcano in metres)	0.06	1500	4×10^{-5}
Gravity (g, in ms^{-2})	9.81	9.81	1
Viscosity (Pa s)	4×10^4	1×10^{11}[a]	4×10^{-7}
Stress (Pa)			2.1×10^{-5}
Strain rate (stress/viscosity)			5.2×10^{1}
Time (viscosity:strain)			1.9×10^{-2}
Velocity (strain rate×length)			2×10^{-3}
Time intrusion	1.33×10^5 s (37.16 h)	5011200 s (58 days)	2.67×10^{-2}
Average incremental fault displacement (m)	4×10^{-6}	0.1	4×10^{-5}
Fault velocity (ms^{-2})	3.99×10^{-11}	1.9×10^{-8}	2×10^{-3}

[a]Alidibirov and Dingwell (1996)

Results

Basal shearing of the cone without intrusion

Sixteen experiments were conducted in which a cone was subjected to basal shear. Similar structures were observed to develop in each case. After movement of the basal plate by approximately 4 mm, instability of the cone developed in regions above the underlying shear. These unstable regions were characterised by the development of oversteepened flanks and fractures. With continued basal shearing, these features developed into persistent landslides on the flanks where the cone had been destabilised. The landslides were oriented in between the R and P shears, slightly oblique (10–20°) from the main strike-slip faultline and towards the side of the R shear. R and P shears are structural terms given to faults characteristic of, but not limited to, strike-slip faulting (Wilcox et al. 1973). R and P shears are synthetic faults that form at acute angles relative to the trend of the main strike-slip faultline. At the stage when oversteeping and development of fractures were fully developed, the motor that rotates the screwjack was stopped and the detailed surface and internal structures were examined.

Structural patterns observed in plan view

The analogue cones invariably developed two sigmoidal structures on their surfaces, herein denoted as sigmoids I and II. Each sigmoid has its long axis positioned at an acute angle relative to the main strike-slip fault direction (Fig. 5). Sigmoid I is outlined by a change in relief of the cone's flank and sigmoid II is defined by cracks (distended fractures). In the acute angle between sigmoids I and II, the flanks get steeper. This bulging is concentrated near to sigmoid I in its concave side, is elongate in appearance, and extends from the base of the cone towards the summit. At the summit, a depression forms within a graben. This graben becomes more pronounced while the unstable regions slip downslope.

The same sigmoidal structures are present both for cones that are deformed by right-lateral and left-lateral strike-slip motion. The positions of these structures depend on the type of shear movement (i.e. left or right-lateral), and are mirror images of each other.

The general features observed in these experiments are like those described by van Wyk de Vries and Merle (1998). These authors were, however, concerned with the effect of volcano loading on the geometry of strike-slip faults cutting weak sedimentary rocks, and they did not consider the faulting on the cone in great detail. Here we are more interested in the structures produced in the cone, and are dealing with cases where there is a rigid substrate.

Internal structural patterns

Vertical cross sections of the cone's interior reveal a flower structure (Fig. 6), bounded on one side by a reverse fault and on the other by a normal fault. The reverse faults start to form near the base of the cone and disappear upon nearing the summit. The normal faults, in contrast, are confined to the central portions of the cone. Reverse faults directly underlie the bulge observed on the surface. Movement along the reverse faults is approximately 1–2 mm. At the summit, graben structures are present (Fig. 6h,i).

Horizontal cross sections at different levels of the cone show two sets of synthetic faults positioned at acute angles relative to the main strike-slip fault direction (Fig. 7). One set occurs roughly parallel to the Reidel, R shear, and the other to the P shear. Those faults, aligned parallel to the R shear, are found in all

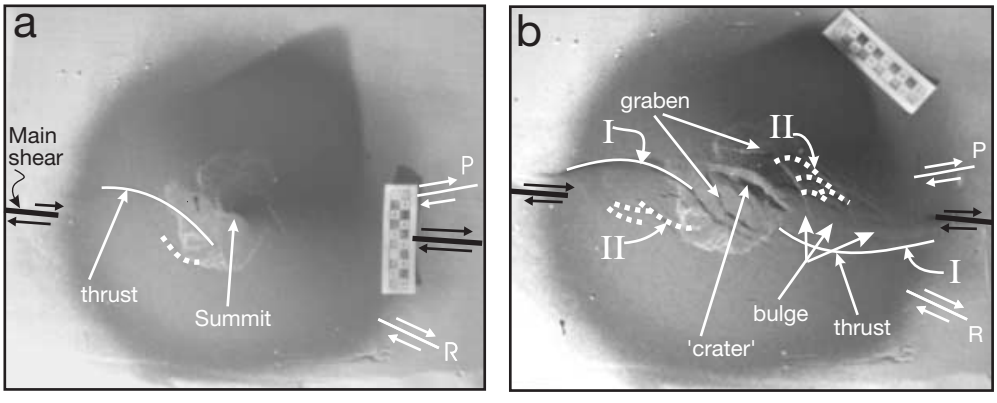

Fig. 5a,b Stages of surface deformation of an analogue cone which is sheared at its base by a right-lateral strike-slip fault. **a** The cone without much deformation. The summit remains pointed and intact. **b** Sigmoidal structures are formed along the flanks of the cone, and are positioned at acute angles relative to the main strike-slip fault direction. Bulging occurs near to sigmoid I in the concave side. The bulge is an effect caused by reverse faulting. A depression develops at the summit and is flanked by a graben. *Square* in the scale bar is equal to 1 cm

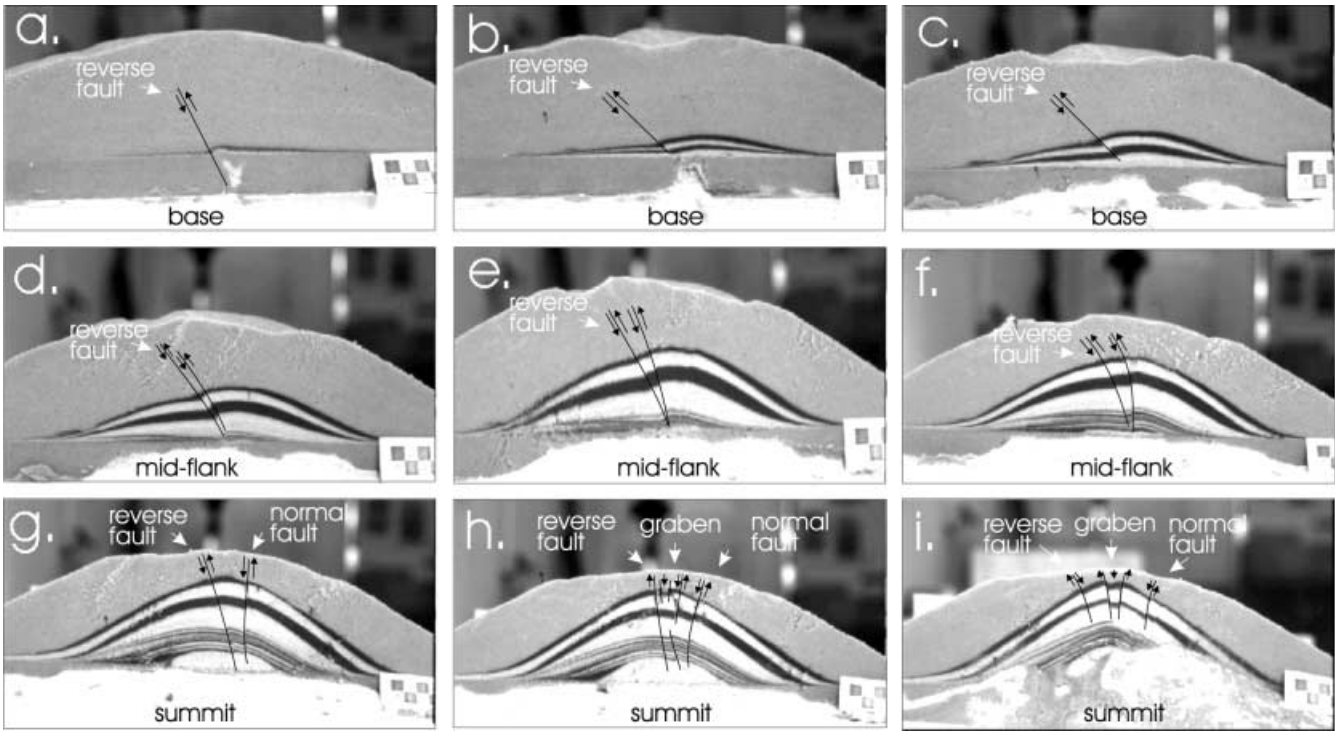

Fig. 6a–i Vertical cross sections of a deformed analogue cone cut perpendicular to the basal shear. Cross sections progressing from cuts near the base of the cone towards the summit. The figures show the development of reverse and normal faults. The opposite side of the cone is a reverse image of structures formed in this portion of the cone (not shown). The topmost layer above the black layer is for protective covering only. It is not part of the analogue cone model. *Square* in the scale bar is equal to 1 cm

Fig. 7a–f Horizontal cross sections of a deformed analogueue cone cut parallel to the basal plate. Deformation of the cone in this example is by right-lateral strike-slip shearing of the basal plate. Progression of horizontal cuts from the summit to the base of the cone. Sets of fault structures are formed nearly parallel to the *R* and *P* shears. Reverse and normal faults are indicated by *triangles* and *thick lines*, respectively. Those formed parallel to the P shears are found mainly at the upper portions. *Square* in the scale bar is equal to 1 cm

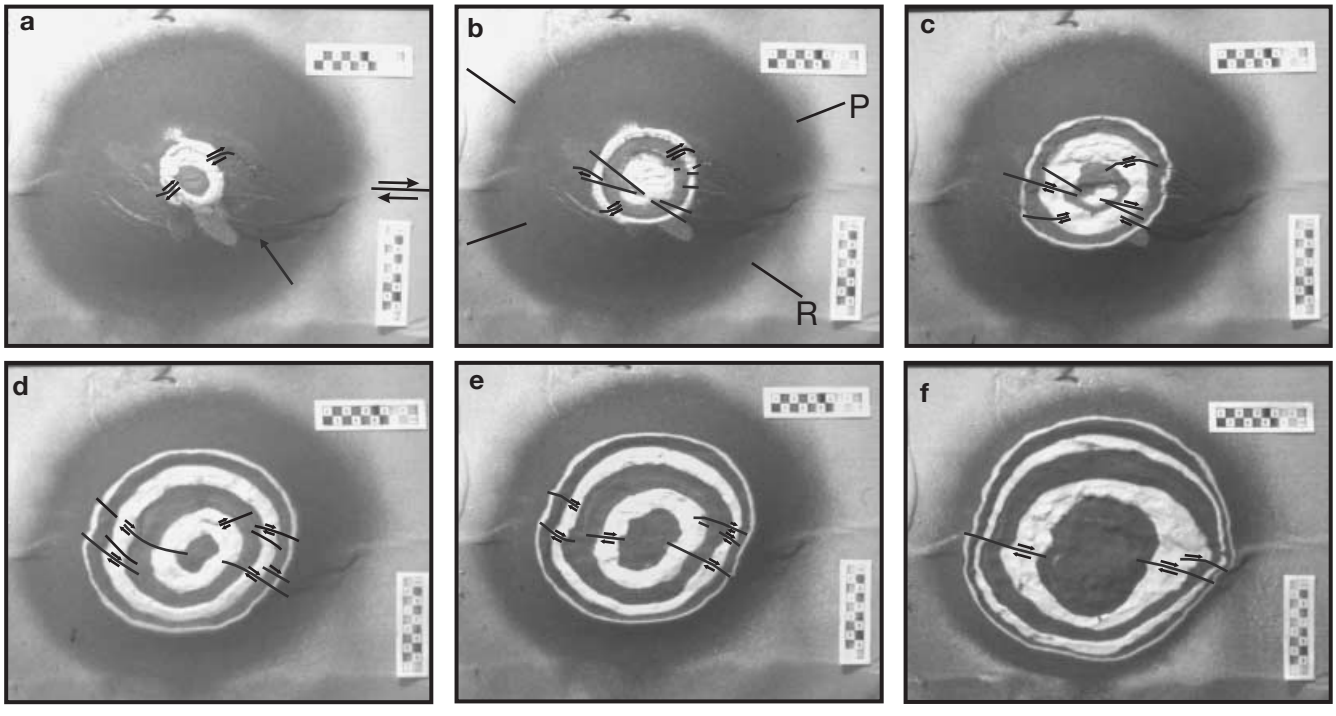

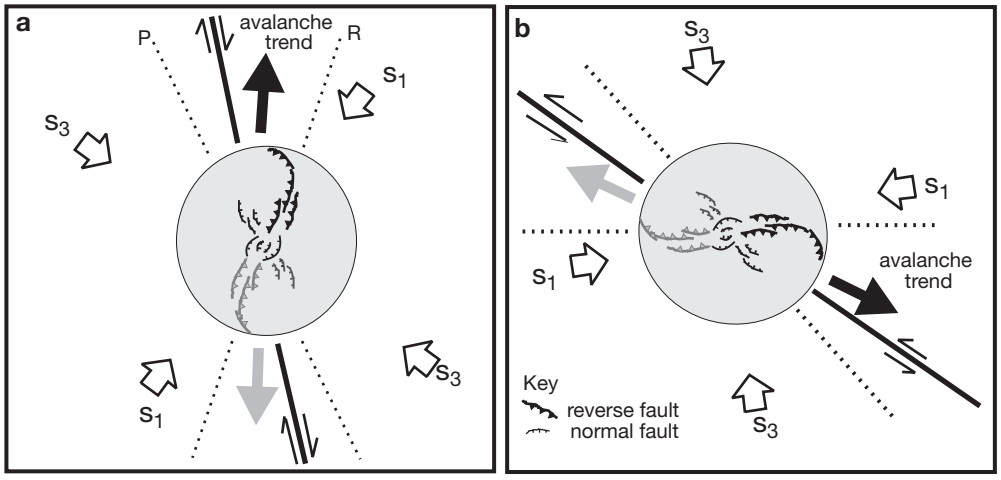

Fig. 8a,b Summary of results and predictive model for cones overlying strike-slip zones. **a** Right-lateral strike-slip fault. **b** Left-lateral strike-slip fault. The structural pattern on one flank is outlined as *black* and those in the diametrically opposite side are outlined as *grey*. They are outlined differently to emphasise inverted structural patterns. σ_1 and σ_3 are, respectively, the maximum and minimum horizontal stress. *P* and *R* are synthetic faults generated at acute angles to the main strike-slip shear

levels of the cone, except for the topmost portions. These faults define an acute angle relative to the main strike-slip fault line, which decreases from the top to the bottom of the cone (i.e. 32° at the upper portions to ca. 16° at the cone's base). The other set of faults is aligned approximately with the synthetic P shear direction. These faults, parallel to the P shear direction, are confined mainly to the mid and upper horizontal sections of the cone. The acute angle defined by these faults relative to the main shear also decreases from upper to lower levels (i.e. from 25 to 18°).

The observations taken altogether form a three-dimensional picture of the deformation inside the cone. Instead of a vertical planar cut along the cone, a set of transpressional and transtensional faults (combined dip-slip and strike-slip movement) flower in its interior. The dip-slip component may be either a normal or a reverse fault. The strike-slip component follows the sense of movement of the main shear. The transpressional and transtensional faults curve in a sigmoidal fashion along a strike defined by the R and P shears with reverse faulting and normal faulting occurring in the R and P shear positions, respectively. The surface expression of these faults is also sigmoidal in form and defines a region of deformation and instability. Bulges and cracks (distended fractures) are characteristic of this unstable region. The bulges are formed in the area above the reverse fault, whereas the cracks are formed on top of the normal faults. The depression at the summit is generated within the graben fault structures.

The geometry and kinematics of deformation found in the cone experiments are invariable, and can be determined by the position and sense of movement of the underlying strike-slip shear. A summary of these results is shown in Fig. 8. A cone subjected to basal shearing generates a region of deformation bounded by transpressional and transtensional faults oriented slightly oblique to the main shear. On the surface, these faults appear as sigmoidal structures denoted as sigmoids I and II. The region defined by the acute angle between sigmoids I and II are areas where persistent landsliding occurs and are highly unstable flanks.

Intrusion models

In all the intrusion experiments, the initial strike-slip motion induced in the cone produced the same structures observed in the first set of models (i.e. basal shearing without intrusion). The results of the intrusion models are given below.

Control experiments

With the control experiments, silicone putty was intruded into a cone, which had not previously been deformed. The same features were observed as those found in the models of Donnadieu and Merle (1998) Merle and Donnadieu (2000). A normal fault and a thrust fault formed above and below the intrusion, respectively, and a bulge developed on the cone's flank. The location of the bulge and structures showed no systematic preferred orientation from one experiment to the next.

Strike-slip before initiating intrusions

In these experiments the cone was deformed by basal shearing prior to intrusion. The behaviour of the intrusion is divided into stages. During the first stage, the intrusion followed a central course within the cone. Fractures were observed forming radially around the top of the cone (Fig. 9a). After injecting approximately 1 cm^3 of silicone (stage 2), the intrusion began to climb up one of the normal faults generated previously by strike-slip movement (Fig. 9b). A bulge appeared in the area of the normal fault trace. With

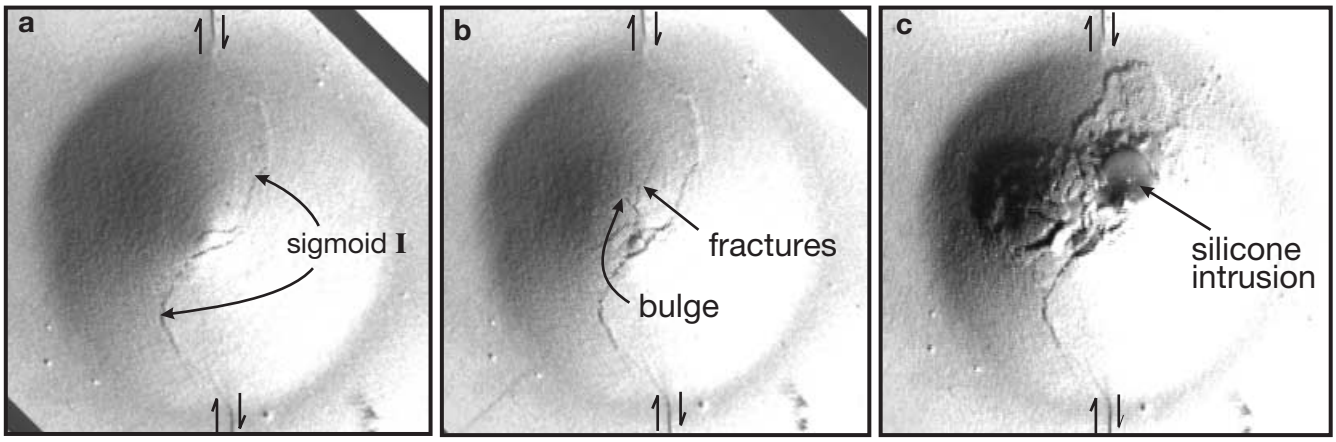

Fig. 9a–c Sequence of events of intrusion experiments. **a** Pre-intrusion shearing. The cone shows deformation structures (sigmoid I). Deformation structures appear after 4 mm of basal shear movement. **b** Cone after 3 h of intrusion. Bulging appears in the concave region of sigmoid I where the reverse faults are situated. **c** Persistent landslides are generated until the intruding silicone penetrates the surface beside the trace of sigmoid I

Fig. 10a–c The effect of cryptodome intrusion into a strike-slip deformed cone. **a** A horizontal section through a cone cut at approximately half height. The pre-intrusion sigmoid I and sigmoid II are indicated as well as the syn-intrusion major shear fault and the lower flank thrust. There are three sequential positions of the silicone intrusion indicated *1*, *2*, and *3*, which are also depicted in **c**. At first the intrusion is in the centre (*1*), then it begins to climb up the normal fault (*2*). At this point there is bulging on the northwest flank. The intrusion then pierces into the fractured area between sigmoids, and travels at an oblique angle. It then forms a new major shear fault (*MSF*) and a lower flank thrust, which both join the sigmoid faults. The bulge grows laterally on the flank. **b** Photograph of a sectioned experiment illustrates the features. Note that this experiment was conducted with an intrusion and strike-slip fault slightly offset to the left of the cone summit. Even with this geometry the intrusion traveled along strike of the main fault. **c** Vertical cross-sectional diagrams of the intrusion made strike-normal and strike-parallel to the main basal strike-slip shear. The cone is 15 cm wide

further intrusion (stage 3), the silicone cut the normal fault trace and entered the region between the normal and reverse faults. Both these faults were then reactivated. The reverse fault maintained its original sense of movement while the normal fault was inverted into a reverse fault. An elongated bulge grew between these faults and was characterised by persistent landsliding until the flank was pierced (Fig. 9c). A diagram showing the internal structure of the volcano after it was pierced is shown in Fig. 10. Intrusion always occurred on the side with the better developed reverse fault system.

Strike-slip motion concurrent with intrusion

Simulation runs using this set-up produced results similar to those obtained from the previous intrusion experiments (i.e. strike-slip before intrusions). The only difference is that a better formed reverse fault was strongly used by the intrusion to push into the cone.

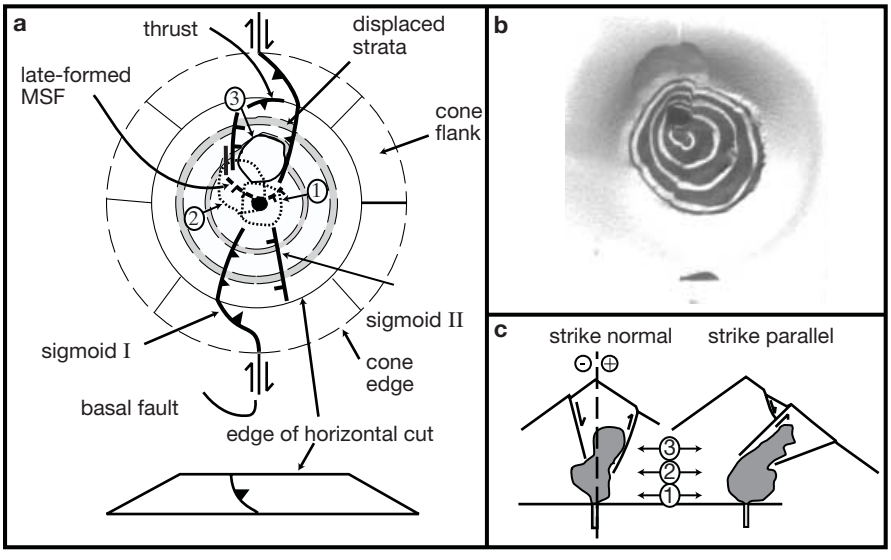

Discussion

The principal features of these analgoue cone experiments show that flanks of volcanoes can become unstable due to basal strike-slip movement. The amount of movement required in the analogue models to generate instability is 4 mm. This is equivalent to approximately 100 m for a natural prototype with cone elevation of 1500 m. Smaller edifices need less amounts of strike-slip displacement for generating instability. For typical rates of strike-slip fault movement of approximately 1 mm $year^{-1}$ to 1 cm $year^{-1}$ (Groppelli and Tibaldi 1999), it would require 10^4–10^6 years (Wadge 1982); thus, it is expected that strike-slip-induced instability would be a common process for volcanoes in certain tectonic settings.

The analogue models describe the geometry and type of structures expected at volcanoes undergoing strike-slip deformation. On actual volcanoes, erosion and emplacement of new volcanic units modifies structures rapidly and can obscure the features produced in the models. Several geometric forms are likely to be produced, however. The sigmoid shape that is so clearly developed in the models is likely to appear. Scarps on the surface of the volcano formed due to faulting may become accentuated by erosion, except if the volcano is resurfaced at a higher rate than the generation of structures by strike-slip deformation. The two sides of the cone aligned with the basal strike-slip fault should have greater relief and have more accentuated erosion. In the lower parts of a cone, they are likely to be buried under clastic deposits. Fracturing over a growing thrust may lead to enhanced erosion, and it is probable that erosion will etch out the trace of the sigmoid. Gullies or valleys produced could form major drainage channels for a cone or, alternatively, they may provide pathways for lava flows and end up as positive relief again.

The detection of the effects of strike-slip faulting is therefore dependent on finding anomalous sigmoid patterns, or specific scarps or erosional forms on the upper flanks that reflect its extension. Knowledge that a volcano lies over a strike-slip fault is then combined with morphological observations to detect the sigmoids. Higher on the cone, the area likely to be occupied by the sigmoid should be inspected for fracturing. Indicators of fracturing may be the presence of vents, previous domes, fumaroles and non-radial erosional gullies. In cases where collapse has occurred, the amphitheatre scar may reveal faults that are aligned approximately parallel to the underlying shear.

The orientation of the destabilised areas of a volcano sheared by basal strike-slip movement lie approximately 10–20° oblique to the trend of the underlying shear towards the side of sigmoid I. These are areas where gravitational sliding and collapse may occur.

In the following sections, the analogue models are compared in detail with the morphology and structures found in Iriga and Mount St. Helens volcanoes. The case studies presented are representative of both structural failure of a volcano without magmatic intrusion, and that which is associated with a cryptodome. These two cases are discussed below.

Iriga volcano

Iriga is a stratovolcano located in southeastern Luzon, Philippines. The debris avalanche of ca. 1628 AD (Aguila et al. 1986) resulted in the removal, transport and deposition of 1.2 km^3 of edifice material covering an area of 70 km^2 southeast of the volcano. The collapse event left behind an elongated amphitheatre with parallel-sided walls. Debris avalanche deposits show no evidence of contemporaneous magmatic activity, suggesting that there was no volcanic trigger for the sector collapse event.

Analysis of synthetic aperture radar (SAR) images of the area of Iriga volcano reveals a prominent lineament that strikes northwest–southeast along the length of the amphitheatre structure (Fig. 11). Drainage patterns found in the SAR images (see Fig. 2) show that this lineament is a left-lateral strike-slip fault. This is part of the Legaspi fault (Aurelio et al. 1997), which extends offshore into the Philippine Sea basin. Focal-point mechanisms of recent earthquakes (Aurelio et al. 1997) also indicate left-lateral displacement. Other notable structural features within the region include a graben south of Iriga, northwest/southeast-striking lineaments, and less prominent northwest/southeast-trending axes are also present south of the SAR image coverage. All these deformational features are consistent with the regional stress field.

The aerial photographs and DEM of Iriga (Fig. 12) reveal numerous striking features similar to those found in the analogue models, which suggest that strike-slip movement may have led to the instability, and subsequent collapse, of its southeast flank. These include: (a) northwest–southeast elongation of the volcano; (b) a narrow parallel-sided amphitheatre; (c) faults parallel to the left-lateral strike-slip shear that cuts the edifice; and (d) strong erosion of the flanks in the direction of the strike-slip trend. Iriga is an elongated volcano with its long axis trending northwest–southeast. This has the same orientation of elongation relative to the basal shear seen in the analogue cone models. An amphitheatre scar is present with its mouth open to the southeast. This scar has the form corresponding to the acute angle defined by sigmoids I and II. Faults observed within this scar from aerial photographs show alignment with the underlying strike-slip trend. Strong erosion affects the flanks diametrically opposite this amphitheatre (Fig. 12). Large gullies on the north and northwest flanks occupy the

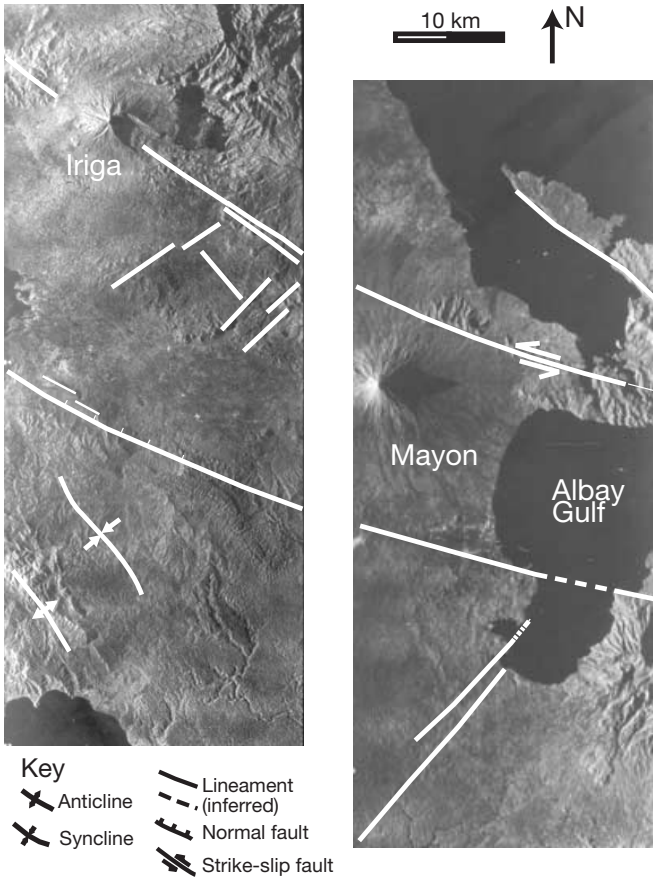

Fig. 11 Synthetic aperture radar images show the tectonic setting of Iriga and Mayon volcanoes. The interpretation of the brittle and plastic deformational structures is consistent with the movement of the Philippine fault to its southwest

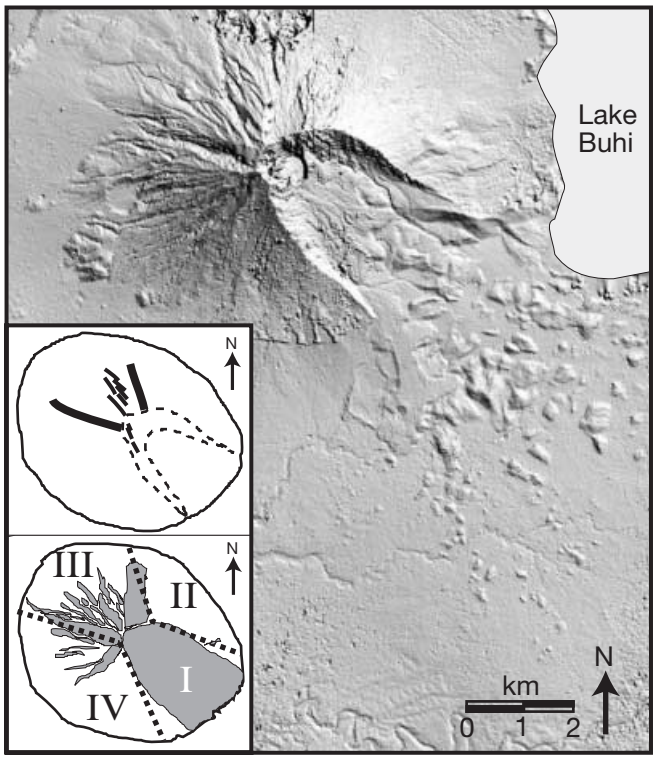

Fig. 12 Digital elevation models (DEM) of Iriga volcano shows the amphitheatre opening and prominent erosional features. *Upper left inset* depicts the positions of the proposed sigmoids and non-radial fractures on the north and northwest flanks. These appear as gullies and erosional features on the DEM. Lineaments that trend parallel to the underlying shear are present within the amphitheatre scarp as observed from aerial photographs. *Lower left inset* is the elongate Iriga cone divided into four sectors. Sector I is the position of the amphitheatre. Opposite the avalanche is sector III, which is strongly eroded. Little erosion is seen in sectors II and IV

positions where sigmoidal fractures are expected and the area between them is more eroded than the adjacent flanks. The northeast and southwest (sectors II and IV in Fig. 12) flanks are characterised by relatively smoother slopes. All these structures are consistent with strike-slip displacement and deformation of Iriga volcano.

According to the analogue experiments, instability develops parallel to the strike-slip trend, indicating areas where structural failure of the Iriga edifice is likely to take place. The unstable reions in the analogue experiments are defined by the formation of a set of normal and reverse faults, and by a graben structure at the summit. The outline of these unstable regions are closely similiar to the plan geometry of the sector-collapse scar and the highly eroded northwest flanks.

Mount St. Helens

Mount St. Helens is a stratovolcano that has suffered several collapse events during its evolution. In the past 20,000 years, it has experienced four episodes of instability that led to collapses: the most recent on 18 May 1980; two at ~2.5 ka (Hausback and Swanson 1990); and another at ~20 ka (Newhall 1982). The three more recent collapses were directed to the north and the ca. 20-ka failure was to the south. No collapses are known to have been directed to the east or west.

Based on the findings from the analogue experiments, we believe that strike-slip faulting and the generation and orientation of the collapse events were related. Movement of the Mount St. Helens shear (see Fig. 2b) develops faults and oversteepening at the northern and southern flanks, creating instability in these areas. Moreover, the faults act as pathways for intruding magma resulting in further destabilisation.

The Mount St. Helens shear was notably active in the years before and after the 1980 collapse event and was responsible for numerous tectonic earthquakes, some as large as magnitude 5. It is ultimately believed to have triggered the 18 May collapse (Endo et al. 1981; Weaver et al. 1981). Activity of this strike-slip

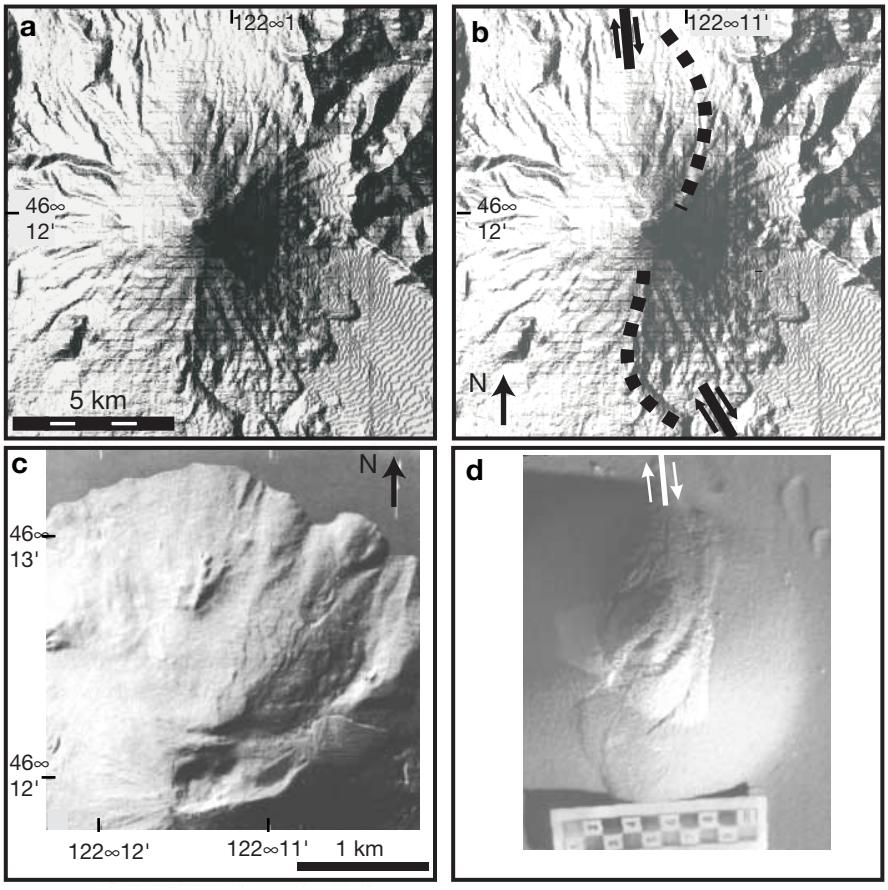

Fig. 13a–d Comparison of the pre-eruption DEMs of Mount St. Helens and the analogue model. **a** Pre-eruption DEM of Mount St. Helens. **b** The DEM with the outline of the right-lateral strike slip and sigmoidal feature. **c** The DEM produced from photographs of 12 and 16 May 1980 shows the crater and fracture patterns (after Jordan and Kieffer 1981). **d** Analogue cone model shows structures which are like those found in **b** and **c**. Strikingly similar features are the sigmoidal structure, position, and direction of strike-slip movement, graben at the summit, elongated bulge and fractures trending slightly northeast, and absence of fracture systems northwest of the edifice

fault may have developed features on Mount St. Helens that closely resemble those generated in the analogue models. On the north and south flanks, there is a sigmoid feature. On the north side, this corresponds to a curving ridge extending from the summit via Dogs Head and around Sugar Bowl. To the south, the lower extension of the sigmoid is defined by a prominent gulley north of Swift Creek (Fig. 13). Analysis of the geologic maps of Mount St. Helens (Crandell 1987) show that these sigmoid structures are not defined by the outline of lava flows (Fig. 14). In some portions, however, the trace of the sigmoid

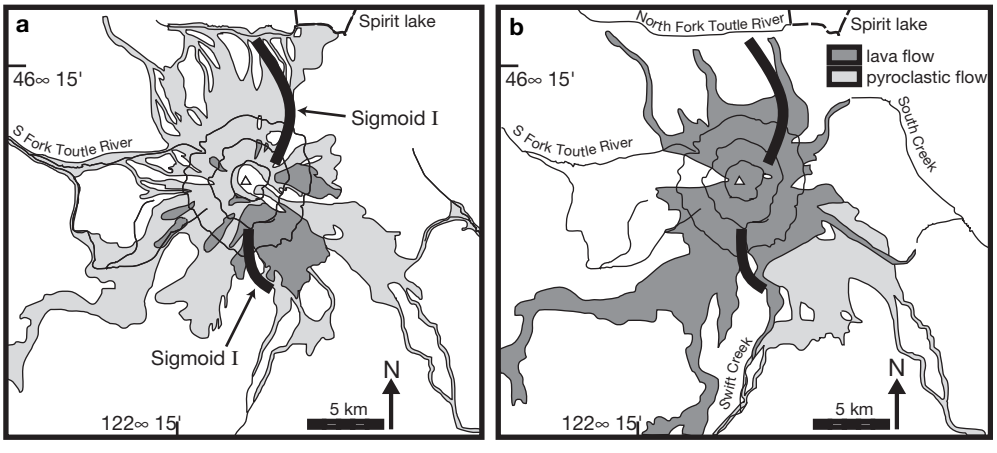

Fig. 14a,b Lava flow and pyroclastic flow distribution maps of Mount St. Helens (Crandell 1987). **a** Kalama age: Shown is the location of the sigmoid structure as observed from DEM and topographic maps. The trace of the sigmoid is not wholly defined by the outline of any deposit. On the upper slopes of the northern flank, the pyroclastic flow deposit follows the trace of the sigmoid as if being topographically constrained. **b** Castle Creek age: again, the trace of the sigmoid does not completely correspond to the outline of any deposit. The tongue of the lava flow bends along the southern extension of the sigmoid

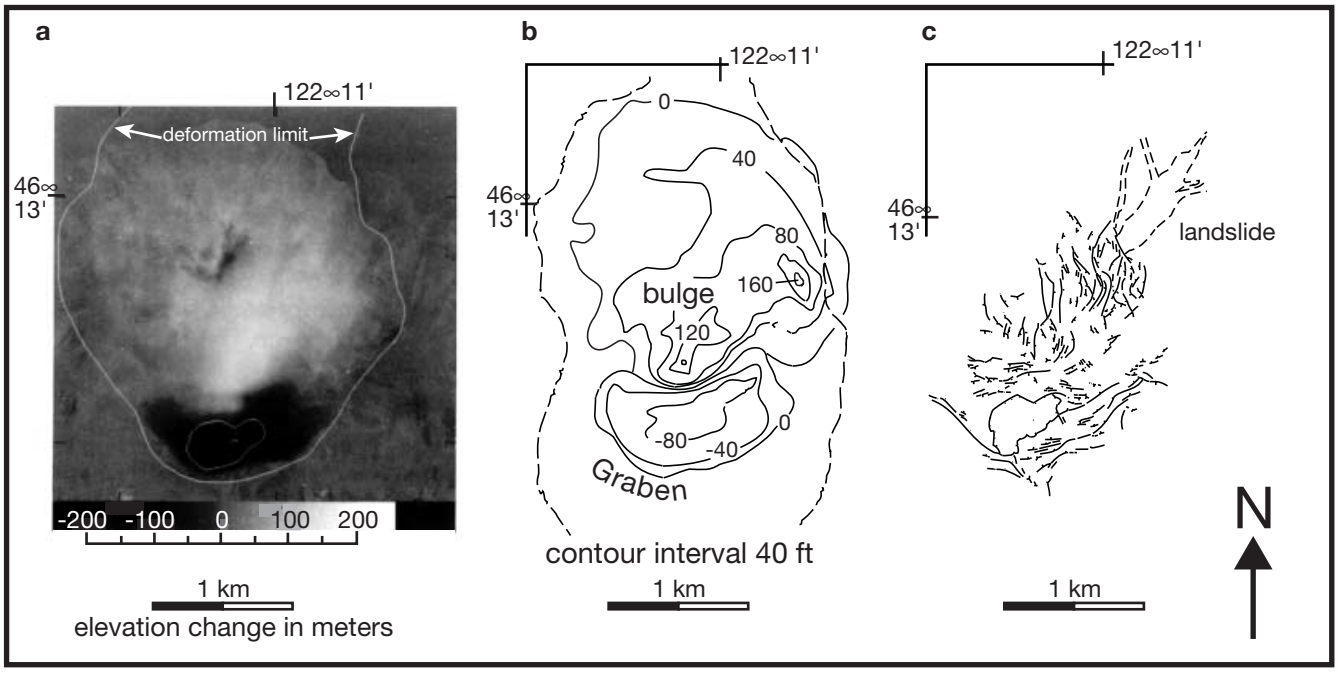

Fig. 15a–c Bulging and fracture patterns in the north flank of the pre-May 1980 edifice of Mount St. Helens. **a** Computer-generated image shows total elevation changes from 1972 to 12–16 May 1980 (after Jordan and Kieffer 1981). **b** Bulging from 12 April to 1 May 1980, represented as contours. The *dashed line* shows the outline of the post-collapse amphitheatre. **c** Fracture pattern of the north flank on 12 May 1980. **b** and **c** are taken from Moore and Albee (1981). Note the north–northeast trend of the bulge and fractures

Fig. 16a–c Diagrams of the bulge and set of fractures noted in the analogue experiments of Donnadieu and Merle (1998) and this study, superimposed on a pre-1980 topographic map of Mount St. Helens. **a** In Donnadieu and Merle's model, the bulge and the fractures are symmetrical. The bulge overlies the intruding 1980 cryptodome and is located in a position as estimated by Moore and Albee (1981). *MSF* refers to the major shear fault that develops ahead of the incipient cryptodome, which subsequently guides the intrusion path. **b** The position of the sigmoids, the bulge and fractures patterns predicted in this study. **c** The actual bulge pattern for comparison. Note the curving nature of the bulge following roughly the trace of sigmoid I. The locations of pre-existing domes are shown in *grey*

appear to guide the flow of lava as well as pyroclastic flows.

In the weeks preceding the 18 May 1980 flank failure, structures were formed on the north flank. These were the elongated bulge to the north–northeast and the fracture system that also trended in the same direction (Fig. 15). These structures are closely similar to those found in the analogue models.

There were several pre-existing domes on the north flank (Crandell 1987) coinciding with the trace of the proposed sigmoids. The Kalama dome occupied the summit, Sugar Bowl dome on sigmoid I (reverse faults) and Goats Rock dome on sigmoid II (normal faults; Fig. 16). The 1980 cryptodome bulge was confined between the proposed sigmoids. The inflation was asymmetrical, with Goats Rock appearing to have a dampening effect on surface deformation, while a curved region of pronounced uplift followed the trace of sigmoid I (refer to Fig. 13b).

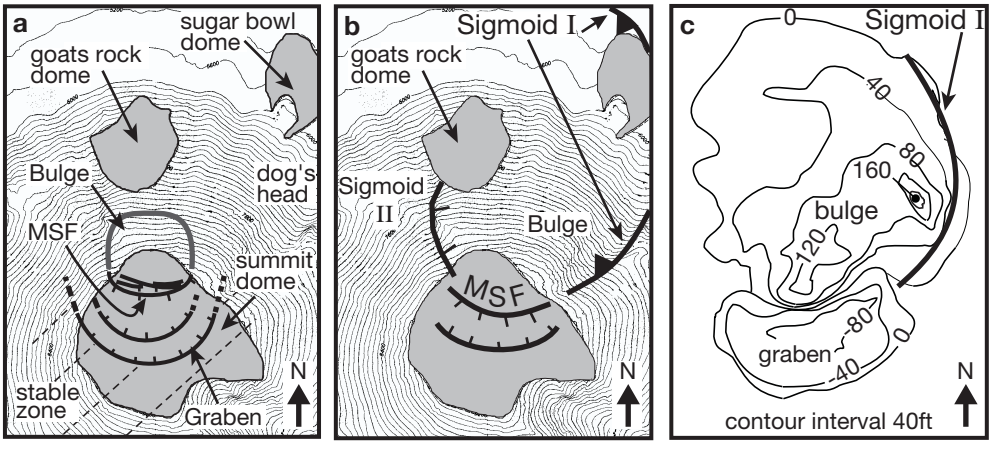

We interpret the instability of the northern flank to be the result of incremental build-up of stress in the ~5-ka (Mullineaux and Crandell 1981) life of the upper elevation cone of Mount St. Helens. Continuous strike-slip activity underneath Mount St. Helens prior to the 1980 collapse event led to fracturing of the flanks above the Mount St. Helens shear. The fractures were preferentially developed on the north flank and later on guided the intruding magma. The magma intruded between pre-existing normal and reverse faults, and activated these structures. This upward movement of magma created the elongated bulge (~60 m; Jordan and Kieffer 1981) and the asymmetrical fracture pattern that were both oriented in a north–northeast direction.

It is well known that the 1980 collapse of Mount St. Helens was strongly controlled by the intrusion path of the 1980 cryptodome (Christiansen and Peterson 1981). The questions that now arise are why it was preferentially intruded in any one direction and how the intrusion relates to the surface fractures formed prior to the collapse event. One possible factor that may have controlled the path of the cryptodome is through formation of a shear ahead of the intruding magma, which subsequently guided the intrusion (Donnadieu and Merle 1998). While the shear did form in all experimens, its location was always controlled by the pre-existing high-angle transpressional and transtensional faults. In the model of Donnadieu and Merle (1998), intrusion occurred in random directions.

The model presented here improves on the previous analogue model of Mount St. Helens by Donnadieu and Merle (1998), since it can explain the directional path of the intrusion and observed patterns of bulge and fracture asymmetry. Pre-stressing and fracturing the Mount St. Helens volcanic edifice by movement of the underlying Mount St. Helens shear formed a set of normal and reverse faults. These dip-slip structures were the sites preferred by the intrusion, and in turn were re-activated. Continuous intrusion of magma formed a cryptodome that was guided by the pre-existing faults. As the intrusion rose along the faults it created a shear fault between the sigmoids I and II, possibly exploiting previous tensional fractures. This resulted in rapid uplift in the region where the reverse faults were located. On the surface, this upheaval was manifested on the northern flank of Mount St. Helens as an elongated bulge and set of fractures that trend north–northeast (Fig. 16). This feature is different from that expected in the model of Donnadieu and Merle (1998), where a symmetrical U-shaped set of fractures form at the margins of the bulge.

Summary and conclusion

Analogue experiments with sheared sand cones have been used to explore the stability of volcanic cones that lie above strike-slip faults. The response of the cone to basal shearing is that a flower structure composed of a complex set of curving transpressional and transtensional faults is produced within the cone. The formation of this set of curving faults generates a defined region of instability, which has an orientation slightly oblique to the strike-slip trend. This unstable region is marked by oversteepening (bulging) and is the product of vertical movement along reverse faults. The faults may develop rapidly or in a slow and incremental manner, depending on the rate of movement of the underlying shear. Once formed, these structures can be used as pathways by rising magma to further destabilise the cone. Based on the analogue models, the rising magma prefers to intrude the region between the reverse and normal faults. These faults are consequently reactivated as reverse faults and create significant upheaval as the magma penetrates toward the surface. The result of continued shearing of the volcanic cone is that the flank becomes destabilised and then, with or without the aid of magmatic intrusion, may be followed by catastrophic collapse of the destabilised volcanic flank.

Model results were compared with two volcanoes underlain by strike-slip faulting. The collapse structure and direction of failure is as predicted by the model presented. This applies to sector collapse events that are related to magmatic intrusion (Mount St. Helens) and tectonic destabilisation (Iriga). Comparison of pre-collapse DEMs and geodetic data of Mouth St. Helens with the analogue models show remarkable similarities of changes in surface morphology such as bulging and development of fracture patterns.

We propose, based on the results of this study, that at Mount St. Helens a combination of basal strike-slip movement and magma intrusion was responsible for the generation of the large amounts of upheaval in the northern flank. Fractures developed during movement of the Mount St. Helens shear generated pathways for the intruding magma, which in turn produced bulging and movement of the northern flank. Failure of the destabilised flank was finally initiated by the magnitude 5 tectonic earthquake at 08:32 h on 18 May 1980.

Our results can be used to identify regions of instability in volcanoes on top of strike-slip faults. Diagnostic features to identify the effects of strike-slip shearing include sigmoid structures composed initially of reverse and normal faults. The area between these faults is highly fractured and forms a topographic bulge. These unstable regions can eventually lead to sector collapse and are a potential hazard. Identification of these unstable regions can be used to predict the likely direction of sector collapse of a volcano and is useful for hazards mitigation.

Acknowledgements This work was funded by the Department of Science and Technology (DOST), Government of the Philippines, and the German Academic Exchange Service (DAAD), Government of Germany. The National Mapping and Resource Information Agency (NAMRIA) of the Philippines provided ground control points and aerial photographs of Iriga volcano. O. Merle, C. Newhall, C. Oppenheimer and B. Dade offered valuable comments on previous versions of the paper. We thank D. Elsworth and K. Siebe for critical reviews.

References

Adiyaman O, Chorowicz J, Kose O (1998) Relationships between volcanic patterns and neotecteonics in eastern Anatolia from analysis of satellite images and DEMs. J Volcanol Geotherm Res 85:17–32

Aguila L, Newhall D, Miller C, Listanco E (1986) Reconnaissance geology of a large debris avalanche from Iriga volcano, Philippines. Philippine J Volcanol 3:54–72

Alidibirov M, Dingwell D (1996) Magma fragmentation by rapid decompression. Nature 380:146–148

Aurelio M, Barrier E, Gaulon R, Rangin C (1997) Deformation and stress states along the central segment of the Philippine Fault: implications to wrench fault tectonics. J Asian Earth Sci 15:107–119

Bahar I, Girod M (1983) Côntrole structural du volcanisme Indonésien (Sumatra, Java-Bali): application et critique de la methode de Nakamura. Bull Soc Géol France 7:609–614

Begét J, Kienle J (1992) Cyclic formation of debris avalanches at Mount St. Augustine volcano. Nature 356:701–704

Belousov A (1996) Deposits of the 30 March 1956 directed blast at Bezymianny volcano, Kamchatka, Russia. Bull Volcanol 57:649–662

Blanchon P, Shaw J (1995) Reef drowning during the last glaciation: evidence for catastrophic sea level rise and ice-sheet collapse. Geology 23:4–8

Borgia A (1994) The dynamic basis of volcanic spreading. J Geophys Res 99:17791–17804

Carracedo J (1994) The Canary islands: an example of structural control on the growth of large oceanic-island volcanoes. J Volcanol Geotherm Res 60:225–241

Christiansen R, Peterson D (1981) Chronology of the 1980 eruptive activity. US Geol Surv Prof Pap 1250:17–30

Crandell DR (1987) Deposits of pre-1980 pyroclastic flows and lahars from Mount St. Helens Volcano, Washington. US Geol Surv Prof Pap 1444:1–95

Day S (1996) Hydrothermal pore fluid pressure and the stability of porous, permeable volcanoes. In: McGuire WJ, Jones AP, Neuberg J (eds) Volcano instability on the Earth and other planets. Geol Soc Lond Spec Publ 110:77–94

Delaney P, Pollard D, Ziony J, McKee E (1986) Field relations between dikes and joints: emplacement processes and paleostress analysis. J Geophys Res 91:4920–4938

Dhont D, Chorowicz J, Yurur T, Forger JL, Kose O, Gundogdu N (1998) Emplacement of volcanic vents and geodynamics of Central Anatolia, Turkey. J Volcanol Geotherm Res 85:33–54

Donnadieu F, Merle O (1998) Experiments on the indentation process during cryptodome intrusions: new insights into Mount St. Helens deformation. Geology 26:79–82

Duffield W, Stieltjes l, Varet J (1982) Huge landslide blocks in the growth of Piton de la Fournaise, La Reunion, and Kilauea volcano, Hawaii. J Volcanol Geotherm 12:147–160

Elsworth D, Voight B (1996) Evaluation of volcano flank instability triggered by dyke intrusion. Geol Soc Lond Spec Publ 110:45–54

Endo E, Malone S, Noson L, Weaver C (1981) Locations, magnitudes, and statistics of the March 20 to May 18 earthquake sequence. US Geol Surv Prof Pap 1250:93–107

Firth C, Stewart I, McGuire W, Kershaw S, Vita-Finzi C (1996) Coastal elevation changes in eastern Sicily: implications for volcano instability. In: McGuire WJ, Jones AP, Neuberg J (eds) Volcano instability on the Earth and other planets. Geol Soc Lond Spec Publ 110:153–168

Francis P, Self S (1987) Collapsing volcanoes. Sci Am 256:72–90

Francis P, Wells A (1988) LANDSAT Thematic Mapper observations of debris avalanche deposits in the Central Andes. Bull Volcanol 50:258–278

Groppelli G, Tibaldi A (1999) Control of rock rheology on deformation style and slip-rate along the active Pernicana Fault, Mt. Etna, Italy. Tectonophysics 305:521–537

Guest J, Duncan A, Chester D (1988) Monte Vulture Volcano (Basilicata, Italy). Bull Volcanol 50:244–257

Hausback B, Swanson D (1990) Record of pre-historic debris avalanches on the north flank of Mount St. Helens: Geosci Can 17:142–145

Jordan R, Kieffer HH (1981) Topographic changes at Mount St. Helens: large-scale photogrametry and digital terrain models. US Geol Surv Prof Pap 1250:135–142

Lipman P, Moore J, Swanson D (1981) Bulging of the north flank before the May 18 eruption: geodetic data. US Geol Surv Prof Pap 1250:143–155

Lopez D, Williams S (1993) Catastrophic volcano collapse: relation to hydrothermal alteration. Science 260:1794–1796

Marzocchi W, Scandone R, Mulargia F (1993) The tectonic setting of Mount Vesuvius and the correlation between its eruptions and the earthquakes of the Southern Appenines. J Volcanol Geotherm Res 58:27–41

McGuire B, Norton G, Sparks R, Robertson R, Young S (1996) Report of the explosive event of 17–18 September 1996. Tech Rep Montserrat Volcano Observatory

McGuire W, Pullen A (1989) Locations and orientation of eruptive fissures and feeder dikes at Mount Etna: influence of gravitational and regional tectonic stress regimes. J Volcanol Geotherm Res 38:325–244

Merle O, Borgia A (1996) Scaled experiments of volcanic spreading. J Geophys Res 101:805–813, 817

Merle O, Donnadieu F (2000) Identation of volcanic edifices by the ascending magma. Geol Soc Lond Spec Publ 174:43–53

Merle O, Vendeville B (1995) Experimental modeling of thin-skinned shortening around magmatic instrusions. Bull Volcanol 57:33–43

Moore J, Albee W (1981) Topographic and structural changes, March to July 1980: photogrammetric data. US Geol Surv Prof Pap 1250:123–134

Moore J, Clague D (1992) Volcano growth and evolution of the island of Hawaii. Geol Soc Am Bull 104:1471–1484

Moriya I (1980) Bandaian eruption and landforms associated with it. In: Collection of articles in memory of retirement of Prof. K. Hishimura, vol 66. Tohoku University, Tokyo, pp 214–219

Mullineaux D, Crandell D (1981) The eruptive history of Mount St. Helens. US Geol Surv Prof Pap 1250:3–16

Munoz N, Charrier R (1996) Uplift of the western border of the Altiplano on a west-vergent thrust system. J South Am Earth Sci 9:171–181

Murray J (1988) The influence of loading by lavas on siting of volcanic eruption vents on Mount Etna. J Volcanol Geotherm Res 35:121–139

Murray J, Voight B (1996) Slope stability and eruption prediction of the eastern flank of Mount Etna. Geol Soc Lond Spec Publ 110:111–114

Nakamura K (1977) Volcanoes as possible indicators of tectonic stress. J Volcanol Geotherm Res 2:1–16

Nakamura K (1982) Why do long rift zones develop better in Hawaiian volcanoes: a possible role of thick oceanic sediments. Bull Volcanol Soc Japan 25:255–267

Newhall C (1982) A prehistoric debris avalanche from Mount St. Helens. Eos Trans Am Geophys Union 63:45

Pasquaré G, Tibaldi A, Atollini C, Cecconic G (1988) Morphometry, spatial distribution and tectonic control of Quaternary volcanoes in northern Michoacan Mexico. Rend Soc Ital Mineral Petrol 43:1215–1225
Ridley W (1971) The origin of some collapse structures in the Canary Islands. Geol Mag 108:477–484
Shteynberg G, Solovyev T (1976) The shape of volcanoes and the position of subordinate vents. Izvestia Earth Phys 5:83–84
Siebert L (1984) Large volcanic debris avalanches: characteristic of source areas, deposits, and associated eruptions. J Volcanol Geotherm Res 22:163–197
Stewart I, McGuire W, Vita-Finzi C, Holmes R, Saunders S (1993) Active faulting and neotectonic deformation on the eastern flank of Mount Etna, Sicily. Z Geomorphol 94:73–94
Swanson D, Duffield W, Fiske R (1976) Displacement of the south flank of Kilauea volcano: the result of forceful intrusion of magma into the rift zones. US Geol Surv Prof Pap 963
Tibaldi A (1992) The role of transcurrent intra-arc tectonics in the configuration of a volcanic arc. Terra Nova 4:567–577
Tibaldi A (1995) Morphology of pyroclastic cones and tectonics. J Geophys Res 100:24521–24535
Van Wyk de Vries B (1988) Geologia de la isla Zapatera, Lago de Nicaragua. Archive, INETER, Managua, Nicaragua
Van Wyk de Vries B, Francis P (1997) Catastrophic collapse at stratovolcanoes induced by gradual volcano spreading. Nature 387:390
Van Wyk de Vries B, Matela RJ (1998) Style of volcano-induced deformation: numerical models of substratum flexure, spreading, and extrusion. J Volcanol Geotherm Res 81:1–18
Van Wyk de Vries B, Merle O (1996) The effect of volcano constructs on rift fault patterns. Geology 24:643–646
Van Wyk de Vries B, Merle O (1998) Extension induced by volcanic loading in regional strike-slip zones. Geology 26:983–986
Van Wyk de Vries B, Kerle N, Petley D (2000) A sector collapse at Casita volcano, Nicaragua. Geology 28:167–170
Ventura G (1994) Tectonics, structural evolution and caldera formation on Vulcano Island (Aeolian archipelago, southern Tyrhennian Sea. J Volcanol Geotherm Res 60:207–224
Vidal N, Merle O (2000) Reactivation of basement faults beneath volcanoes: a new model for flank collapse. J Volcanol Geotherm Res 99:9–26
Voight B, Elsworth D (1997) Failure of volcano slopes. Geotechnique 47:1–31
Wadge G (1982) Steady-state volcanism: evidence from histories of polygenetic volcanoes. J Volcanol Geotherm Res 87:4035–4049
Weaver C, Grant W, Malone S, Endo E (1981) Post-May 18 seismicity: volcanic and tectonic implication. US Geol Surv Prof Pap 1250:109–122
Weaver C, Grant W, Shemeta J (1987) Local crustal extension at Mount St. Helens, Washington. J Geophys Res 92:10170–10178
Weinberg R (1992) Neotectonic development of western Nicaragua. Tectonics 11:1010–1017
Wilcox R, Harding T, Seely D (1973) Basic wrench tectonics. Am Assoc Petrol Geol Bull 57:74–96